中国光学（中英文）
Chinese Optics
核心期刊

Numerical simulations on the photoelectric performance of AlGaN-based ultraviolet VCSELs with a slope-shaped p-type layer

Wen Xin-xin, JIA Wei, ZHAI Guang-mei, DONG Hai-liang, ZHAO Chao, LI Tian-bao, XU Bing-she

Citation:
Wen Xin-xin, JIA Wei, ZHAI Guang-mei, DONG Hai-liang, ZHAO Chao, LI Tian-bao, XU Bing-she. Numerical simulations on the photoelectric performance of AlGaN–based ultraviolet VCSELs with a slope–shaped p–type layer[J]. *Chinese Optics*, In press. doi: 10.37188/CO.EN–2024–0027
文欣欣, 贾伟, 翟光美, 董海亮, 赵超, 李天保, 许并社. 基于渐变p型层的AlGaN紫外VCSEL外延结构设计和光电性能研究[J]. 中国光学, 优先发表. doi: 10.37188/CO.EN–2024–0027

View online: https://doi.org/10.37188/CO.EN–2024–0027

Articles you may be interested in

A study on the epitaxial structure and characteristics of high–efficiency blue silicon photodetectors
高效率蓝光硅光探测器外延结构及特性研究
Chinese Optics. 2022, 15(3): 568   https://doi.org/10.37188/CO.2021–0188

Research progress of high–speed vertical–cavity surface–emitting laser in CIOMP
长春光机所高速垂直腔面发射激光器研究进展
Chinese Optics. 2022, 15(5): 946   https://doi.org/10.37188/CO.2022–0136

Fabrication and characterization of an LED based on a GaN–on–silicon platform with an ultra–thin freestanding membrane in the blue range
电致发光的完全悬空超薄硅衬底氮化镓基蓝光LED器件的制备与表征
Chinese Optics. 2021, 14(1): 153   https://doi.org/10.37188/CO.2020–0148

Design of a graphene–based wide–band circular polarized antenna for capsule endoscopes
用于胶囊内窥镜的宽频圆极化石墨烯天线设计
Chinese Optics. 2021, 14(5): 1169   https://doi.org/10.37188/CO.2021–0005

Optical design of a wide–spectrum ultraviolet imager based on a single material
基于一种透镜材料的宽谱段紫外成像仪光学设计
Chinese Optics. 2022, 15(1): 65   https://doi.org/10.37188/CO.2021–0127

A review of the effect of GaN–Based Micro–LED sidewall on external quantum efficiency and sidewall treatment techniques
氮化镓基Micro–LED侧壁对外量子效率的影响及侧壁处理技术综述
Chinese Optics. 2023, 16(6): 1305   https://doi.org/10.37188/CO.2023–0091

文章编号　2097-1842(xxxx)x-0001-11

Numerical simulations on the photoelectric performance of AlGaN-based ultraviolet VCSELs with a slope-shaped p-type layer

Wen Xin-xin[1], JIA Wei[1,2]*, ZHAI Guang-mei[1], DONG Hai-liang[1], ZHAO Chao[1], LI Tian-bao[1], XU Bing-she[1,2,3]

(1. *Key Laboratory of Interface Science and Engineering in Advanced Materials Ministry of Education*, *Taiyuan University of Technology*, *Taiyuan* 030024, *China*;
2. *Shanxi-Zheda Institute of Advanced Materials and Chemical Engineering*, *Taiyuan* 030001, *China*;
3. *Institute of Atomic and Molecular Science*, *Shaanxi University of Science and Technology*, *Xi'an*, 710021, *China*)

* *Corresponding author*, *E-mail*: *jiawei@tyut.edu.cn*

Abstract: Owing to the low p-type doping efficiency of GaN-based ultraviolet (UV) vertical-cavity surface-emitting laser (VCSEL) hole injection layers (HILs), effective hole injection in multi-quantum wells (MQW) is not achieved, significantly limiting the photoelectric performance of UV VCSELs. By improving hole injection efficiency, the hole concentration in the HIL is increased, and the hole barrier at the electron barrier layer (EBL)/HIL interface is decreased. This minimises the hindering effect of hole injection. In this study, we developed a slope-shaped HIL and an EBL structure in AlGaN-based UV VCSELs. A mathematical model of this structure was established using a commercial software, photonic integrated circuit simulator in three-dimension (PICS3D). We conducted simulations and theoretical analyses of the band structure and carrier concentration. Introducing polarisation doping through the Al composition gradient in the HIL enhanced the hole concentration, thereby improving the hole injection efficiency. Furthermore, modifying the EBL eliminated the abrupt potential barrier for holes at the HIL/EBL interface, smoothing the valence band. This improved the stimulated radiative recombination rate in the MQW, increasing the laser power. Therefore, the sloped p-type layer can enhance the optoelectronic performance of UV VCSELs.

Key words: UV VCSEL; AlGaN; polarisation doping; EBL; hole injection efficiency

---

收稿日期:2024-08-28; **修订日期**:xxxx-xx-xx

基金项目:中文基金

This work was supported by the Shanxi-Zheda Institute of Advanced Materials and Chemical Engineering (No. 2021SX-AT002 and No. 2022SX-TD018); the Key R & D Projects in Shanxi Province (No. 202302150101012); and the National Natural Science Foundation of China (Nos. 61604104, No. 21972103, No. 61904120).

基于渐变 p 型层的 AlGaN 紫外 VCSEL 外延结构设计和光电性能研究

文欣欣[1], 贾　伟[1,2*], 翟光美[1], 董海亮[1], 赵　超[1], 李天保[1], 许并社[1,2,3]
（1. 太原理工大学新材料界面科学与工程教育部重点实验室, 山西太原 030024;
2. 山西浙大新材料与化工研究院, 山西太原 030001;
3. 陕西科技大学原子与分子科学研究所, 陕西西安 710021）

摘要: 由于 GaN 基紫外 VCSEL 中的空穴注入层 p 型掺杂效率较低, 导致多量子阱中不能实现有效空穴注入, 这极大的降低了紫外 VCSEL 的光电性能。因此本文设计了一种基于 AlGaN 的 UV VCSEL 中使用渐变 HIL 和 EBL 结构。该结构能够提高空穴注入效率, 使空穴注入层中的空穴浓度增加, 也能够使电子阻挡层和空穴注入层界面处的空穴势垒高度降低, 从而利于空穴注入。我们使用商用软件 PICS3D 构建了该结构, 并对能带结构以及载流子浓度等进行了模拟和理论分析。通过空穴注入层 Al 组分渐变引入极化掺杂增加空穴浓度从而提高空穴注入效率。在此基础上电子阻挡层渐变消除了空穴注入层和电子阻挡层界面的空穴突变势垒, 使价带更平滑。这提高了多量子阱中的受激辐射复合速率, 增强了激光功率。因此, 渐变的 p 型层设计可以提升紫外 VCSEL 的光电性能。

关　键　词: 紫外 VCSEL; AlGaN; 极化掺杂; 电子阻挡层; 空穴注入效率
中图分类号: TN248.4　　**文献标志码:** A　　**doi:** 10.37188/CO.EN-2024-0027　　**CSTR:** 32171.14.CO.EN-2024-0027

1 Introduction

GaN-based vertical-cavity surface-emitting lasers (VCSELs) have recently gained increasing attention because of their excellent optical and electrical properties. These include a low threshold current, narrow linewidth, high brightness, and exceptional directionality[1]. These properties make VCSELs ideal light sources for various applications, including optical communication, three-dimensional sensing, and new boosting virtual reality/augmented reality (VR/AR) systems[2]. Significant progress has been made in the structural design of blue-GaN-based VCSELs. For example, Zhang et al. designed a blue VCSEL with a lateral optical confinement structure, exhibiting a threshold current of 16 mA and a maximum optical output power of 0.2 mW[3]. The blue VCSEL designed by Elafandy et al., which utilised birefringent nano-porous distributed Bragg reflectors (DBRs), exhibited a forward voltage of 6 V, differential resistance of 41 Ω, and threshold current density of 59 kA/cm^2[4]. The blue VCSEL developed by Elafandy et al., which employed nano-porous GaN, featured a threshold current density of 42 kA/cm² and a maximum optical output power of 0.17 mW[5]. Hayashi et al. designed a device with a full-width-at-half-maximum divergence angle of 3.9° for an 8-µm-aperture VCSEL with a curved mirror. This performance was observed when the device was operated at a current that was 1.2 times the threshold current (I_{th})[6]. However, compared with blue GaN-based VCSELs, progress in ultraviolet (UV) AlGaN-based VCSELs has been slow. Leonard investigated a 405 nm VCSEL with a threshold current density of approximately 3.5 kA/cm^2[7]. Zhao et al. found that the threshold current density of a InGaN near-UV LD with the n-side down on a submount was 1.27 kA/cm^2[8]. Yang et al. observed that the threshold current of a ridge waveguide-structure UV LD operating under pulsed conditions was approximately 25 kA/cm^2[9]. Zheng et al. proposed a UV VCSEL structure that employed epitaxial lateral overgrowth to prepare high-quality AlGaN multi-quantum wells (MQWs); this structure exhibited a minimum threshold power

density of 0.79 mW·cm^{-2}[10]. The poor performance of UV VCSELs is caused by their low hole-injection efficiency and electron leakage[11].

Numerous methods have been proposed to improve the hole injection efficiency. Qiu et al. designed a p-GaN/n-GaN/p-GaN (PNP-GaN) current-spreading layer[12]. In this design, the thickness of the optically absorptive indium tin oxide (ITO) current-spreading layer can be reduced to decrease internal loss and increase lasing power. Han et al. constructed p-AlGaN/p-GaN hole injection layers (HILs) that improved the electric field within p-GaN and reduced the valence band barrier height of the p-doped electron barrier layer (EBL)[13]. Polarisation doping based on HIL Al-composition gradient has also been used to improve the hole injection efficiency[14-16]. Compared to AlGaN layers with a fixed Al composition, those with a graded Al composition along the growth direction facilitate (1) the generation of high-density electrons and holes through polarisation-induced doping and (2) the manipulation of carrier transport behaviour via energy band modulation[17]. A graded Al composition in p-AlGaN can increase the concentration of polarisation-induced holes and negative-net polarisation charges[18]. Combining the unique composition of the AlGaN structure with such grading creates a channel for polarisation-induced two-dimensional electron gases (2DEGs)[19]. The high ionisation energy of Mg acceptors in AlGaN materials results in low p-type conductivity. Hence, polarisation doping is necessary to form a p-type conduction layer. For Ga face growth, n-type conductivity is achieved by increasing the Al content in the growth direction, and p-type conductivity is achieved by decreasing the Al content[20]. Therefore, the forward resistance and conducting voltage can be reduced by employing polarisation doping to realise p-type conductivity. This minimises a considerable part of the valence-band discontinuity (that is, hole traps).

Electron leakage is a critical factor that affects the optoelectronic performance of VCSELs. Although the EBL can prevent electron leakage, discontinuity in the valence band between the EBL and the HIL can hinder hole injection. Lowering the height of the hole potential barrier can improve hole transport to reduce the hole-blocking effect of the EBL[21-23]. Various EBL designs have been developed to facilitate hole injection, including gradient EBL[24], superlattice EBL[25-26], and staircase EBL[27-28]. The combination of slope-shaped EBL and HIL can also promote carrier injection. However, the growth processes of superlattices and staircase EBLs are complex. Consequently, it is crucial to consider both the influence of the EBL on electron leakage and hole injection, as well as the feasibility of actual production, when designing the EBL.

In this study, we proposed that combining the Al-composition gradient HIL structure with the Al-composition gradient EBL in VCSELs can increase hole injection efficiency and decrease electron leakage. Four different structures were designed to verify the influence of this structure on the device performance: a uniform Al-composition HIL and EBL, gradient Al-composition HIL, gradient Al-composition EBL, and hybrid gradient Al-composition HIL and EBL. We investigated the combined effects of polarisation doping and Al composition gradient in the EBL on the carrier concentration, effective barrier height, stimulated emission, and other performance factors. Combining the gradient Al compositions in the HIL and EBL not only improved hole injection efficiency and smoothened the valence band, but also enhanced the ability to prevent electron leakage. This combination significantly increased the stimulated radiative recombination rate in the quantum, resulting in an increase of 17.8% in laser power, and achieved superior optoelectronic performance.

2 Simulation and calculation methods

Figure 1 illustrates the structure of a GaN-

based VCSEL. The cavity length thickness d_1 of the GaN-based VCSEL device designed in this study satisfied $d_1=\lambda_0/2n$, and the physical thickness d_2 of each DBR layer satisfied $d_2=\lambda_0/4n$, where λ_0 is the lasing wavelength of 375 nm, and n is the real refractive index at the lasing wavelength. The GaN-based VCSEL device consisted of 12 pairs of HfO_2/SiO_2 top DBR and 13 pairs of HfO_2/SiO_2 bottom DBR, sandwiching a cavity with a length of 1.5λ. The cavity of VCSEL A was composed of an ITO layer with a thickness of 20 nm, a p-$Al_{0.12}Ga_{0.88}N$ layer with a doping concentration of 5×10^{19} cm^{-3}, a thickness of 144 nm, a p-type $Al_{0.2}Ga_{0.8}N$ electron-blocking layer (p-EBL) with a thickness of 20 nm, and a doping concentration of 7×10^{19} cm^{-3}. The active region consisted of five pairs of GaN (10 nm)/$In_{0.05}Ga_{0.95}N$ (6 nm) and an n-$Al_{0.12}Ga_{0.88}N$ layer with a doping concentration of 1×10^{19} cm^{-3} and thickness of 177 nm. The main difference between VCSEL B and VCSEL A lay in the fraction of Al within the HIL, which was fixed at 0.12 for the former, whereas it uniformly ranged from 0.06 to 0.18 for the latter. VCSEL C differed from VCSEL A in that the original Al composition of 0.2 in the EBL structure was changed to a uniformly graded Al composition ranging from 0.18 to 0.22. Structure D combined the changes in the HIL and EBL from structures B and C, respectively. All the designed VCSELs used SiO_2 layers for hole current and light confinement. The radii of the bottom and top DBRs were 5 and 3 μm, respectively. The width of the annular electrode was 1 μm. A ring-shaped P electrode was placed above the ITO, and a ring-shaped N electrode was placed above the n-AlGaN, both of which achieved Ohmic contacts.

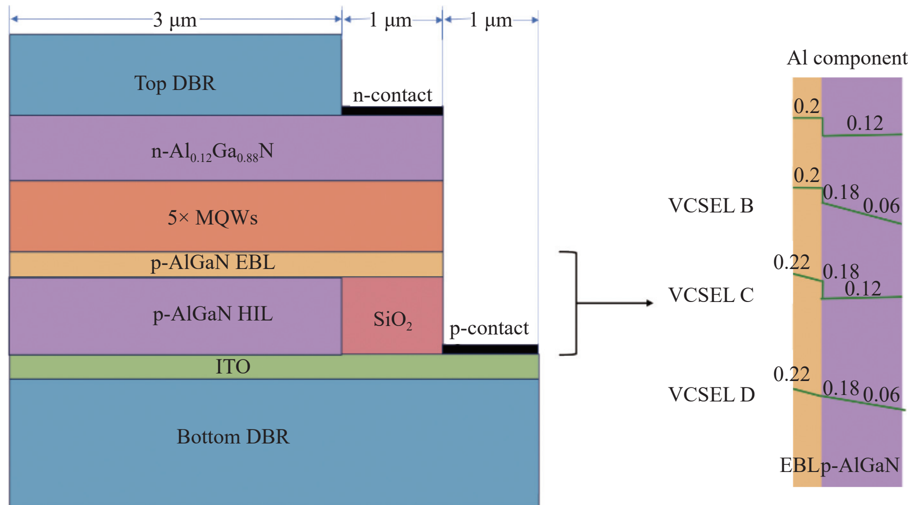

Fig. 1 Structure of GaN-based VCSELs

The simulations in this study were conducted using Crosslight PICS3D, and appropriate boundary conditions were set to solve the Poisson, drift-diffusion transport[29], and rate equations and simulate the electrical and optical characteristics of the device[30]. This model represents a good compromise in terms of efficiency, simplicity, and practical simulation results. In contrast, quantum models based on atomic simulations are more accurate but computationally more burdensome[31]. The absorption coefficients of the materials in the layer were set as follows to ensure that the simulation and experimental results were consistent: ITO at 4012 cm^{-1}, HIL at 70 cm^{-1}, EBL at 70 cm^{-1}, and n-AlGaN at 5 cm^{-1}[32]. The ratio of the InGaN/GaN MQW conduction band step to the valence band step was set to 70/30[33]. The laser operated in a continuous wave mode. The Auger coefficient and Shockley–Read–Hall (SRH) recombination lifetime were set to 2×10^{-31} cm^6s^{-1} and 1×10^{-7} s, respective-

ly[32]. A polarisation level of 40% was considered to reflect the polarisation-induced charges in modelling the spontaneous and piezoelectric polarisations at the lattice-mismatched interfaces[34]. The effective index method (EIM) was used to calculate the optical model of the device, which is suitable for complex structures with oxide-limited apertures[35].

3 Results and discussion

The I-V and L-I curves are shown in Figure 2. Structures B and D exhibited lower series resistances and threshold voltages than structures A and C. The lasing power of all four structures increased with the injection current. All structures began to exhibit an output at an injection current of 0.35 mA. However, the output power at this point was relatively low. It was not until the injection current reached approximately 0.72 mA, corresponding to a current density of 2.55 kA/cm^2, that the output power began to increase significantly. Based on the data, the threshold current of structure D was slightly lower than those of structures A, B, and C. When the injection current exceeded 0.75 mA, the output power of all four structures increased significantly. These simulation results indicate that, despite the similarity of the threshold currents for the four structures, their slope efficiencies differ. Structure D exhibited the highest slope efficiency (0.198 W/A), whereas structures A, B, and C had slope efficiency values of 0.183, 0.187, and 0.194 W/A, respectively.

At an injection current of 20 mA, the output power values for structures A, B, C, and D were 2.87, 3.05, 3.24, and 3.38 mW, respectively. Structures B, C, and D exhibited significantly higher output power than structure A. Specifically, structure D exhibited the highest lasing power, which was approximately 17.8% higher than that of structure A. Eqs. (1) and (2) express the threshold current and emission power formulas for VCSELs, respectively:

$$I_{th} = \frac{eV_a}{\eta_a}(AN_{th} + BN_{th}^2 + CN_{th}^3) \quad , \qquad (1)$$

$$P = \eta_d \frac{hv}{e}(I - I_{th})P = \eta_d \frac{hv}{e}(I - I_{th}) \quad , \qquad (2)$$

where e is the electron charge, V_a is the active region volume, η_a is the carrier injection efficiency, A, B, and C are the SRH, radiative, and Auger recombination rates, respectively, η_d is the differential quantum efficiency thickness, hv is the photon energy, I is the operating current, I_{th} is the threshold current, and P is the emission power. Based on Eqs. (1) and (2), as the carrier injection efficiency increases, the threshold current decreases, and the emission power increases.

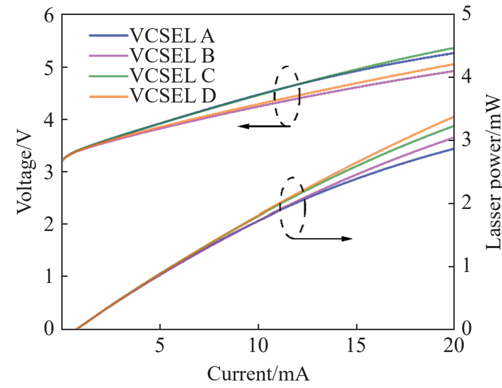

Fig. 2 I-V and L-I characteristic plots of GaN-based VCSELs at 20 mA

Based on the previous analysis, the lasing power has a close relationship with the carrier injection efficiency, whereas the hole injection efficiency has a close relationship with the hole concentration. Hence, the effects of changes in the HIL and EBL on hole concentration were analysed.

Figure 3 illustrates the effects of the different gradient Al fractions of the HIL and EBL on the hole injection efficiency. Figure 3(a) shows the radial hole concentration at an injection current of 20 mA. Compared to structure A, when structure B introduced polarisation doping, it exhibited a significant increase in hole concentration in the active region. Furthermore, while blocking electron leakage, the traditional EBL prevents hole injection[36]. In addition to improving p-type conductivity, the polar-

isation-induced-graded p-type AlGaN layer facilitates electron blocking without introducing additional barrier carriers to hole injection. It also provides extended flexibility in graded-refractive-index design, which is applicable to UV lasers[37]. Under the condition of an unchanged average Al composition, the gradient Al composition of the HIL reduces the abrupt hole barrier at the HIL/EBL interface, thereby weakening the hindrance effect on hole injection. Modifying the EBL in structure C significantly impedes electron leakage and facilitates hole injection. This is because it reduces the abrupt potential barrier at the interface between the HIL and the EBL. Moreover, inhibition of electron leakage is advantageous for hole injection. With the introduction of both polarisation doping and a modified EBL, structure D exhibited the highest hole concentration in the active region. This is attributed to the low ionisation energy of Mg within GaN and the strong interface polarisation charge of AlGaN compounds. The introduction of polarisation doping enables the incorporation of a bulk polarisation charge to increase the hole concentration. Furthermore, because the unshielded polarisation charges at the interfaces are positive, they electrostatically contribute to the appearance of parasitic hole-blocking layers. Therefore, hole injection into the active region is restricted because of the thermionic emission from the hot electrons. However, improving the EBL to address electron leakage issues also alleviate this problem, further suppressing unintentional hole-blocking layers and improving hole injection efficiency.

The hole concentration previously mentioned was determined under dynamic equilibrium conditions. This indicates that at the same injection current and operating temperature, the active region of structure D accumulates more holes than structures A, B, and C. Thus, a higher hole injection efficiency is obtained in structure D, facilitating population inversion and satisfying the threshold conditions for stimulated emissions.

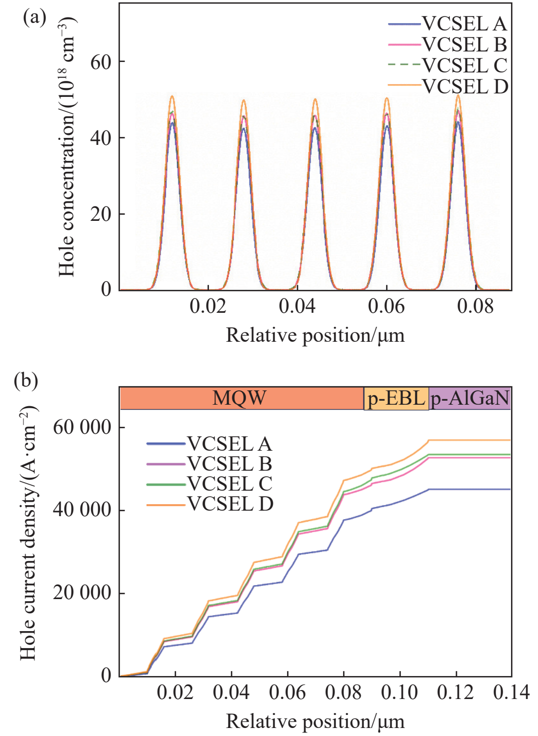

Fig. 3 (a) Radial hole concentrations in MQWs and (b) radial hole current densities for different structures at 20 mA

Figure 3(b) depicts the radial hole current density for each structure at an injection current of 20 mA. The radial hole current density across the active region and p-type spacer layers is higher in structures B, C, and D than in structure A. This demonstrates that polarisation doping improves the ionisation efficiency of Mg dopants, increasing the hole concentration. The longitudinal hole current densities in both the active region and p-type spacer layers of structure D were the highest among all the structures. This further confirms that the combination of gradient Al composition in the HIL and an EBL that effectively blocks electron leakage results in an increased number of holes being injected into the active region, increasing injection efficiency.

Figure 4(a) shows the electron concentration distribution for each structure. A significant electron leakage was observed even in structure A with the EBL. This is caused by the interface polarisation charges between the last quantum barrier and the EBL, as well as between the HIL and the EBL. The influence of the EBL on hole and electron

transport is primarily attributed to the parasitic inversion layer formed by interface polarisation charges and the impact of the active region on the confined carrier density in the EBL. The introduction of polarisation doping and the transition of the EBL to a gradient Al composition resulted in a significant increase in the electron concentration in the active region. Moreover, the combination of these two factors resulted in the highest electron concentration in the active region. This is because the increased hole concentration generated by polarisation doping reduces electron leakage, and the HIL acts as a natural electron barrier to enhance the effective barrier for electrons.

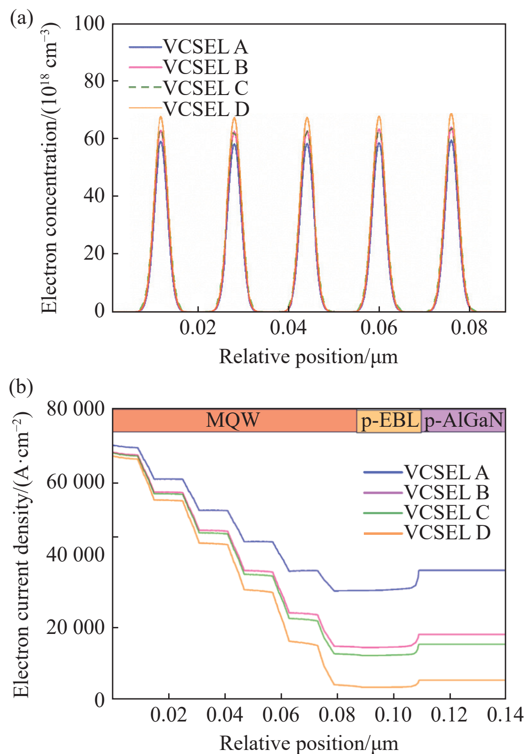

Fig. 4　(a) Radial electron concentration distributions of MQWs and (b) radial electron current density distributions in different structures at 20 mA

Figure 4(b) shows the electron current density distribution on the p-side of each structure. The electron current density exhibited a stair-step trend in the active region, caused by the transport of electrons among the QWs. In each QW, electrons and holes recombined to emit light. Therefore, as electrons passed through each QW, some electron-hole pairs recombined, resulting in a decrease in the electron current density. Electrons injected from the n-type layer into the active region recombined with the holes in the QWs. However, several electrons also spilled over to the p-type layer without undergoing recombination with the holes in the QWs, which is defined as electron leakage. Therefore, the electron current density in the p-type layer can be used to assess the extent of electron leakage. The electron leakage density was significantly lower in structure D, indicating the lowest electron spillover from the active region to the p-type layer (Figure 4(b)). Structures B and C exhibited lower electron leakage densities in the p-type layer compared to structure A. This suggests that structures B and C can also reduce electron leakage. The reduction in the electron leakage density in the p-type layer also suppresses the nonradiative recombination between electrons and holes, increasing the concentration of holes injected into the active region.

Figure 5 shows the stimulated recombination rates in the active region for the different structures. The stimulated radiation recombination rates of structures B, C, and D were all higher than that of structure A. This is closely related to the increased hole-injection efficiency and enhanced ability to block electron leakage. More electron-hole pairs did not undergo nonradiative recombination in the HIL; instead, radiative recombination occurred in the active region. In structure D, the stimulated radiation recombination rate significantly increased near the EBL QW, indicating that more holes were consumed because of the stimulated radiation recombination in the QW.

The wall-plug efficiency (WPE) is a key parameter for evaluating the performance of VCSELs. Figure 6 shows the relationship between the WPE and the injection current. Compared to structure A, all the other structures exhibited improved WPE, consistent with the analysis of the variation in the applied voltage and laser power with the injection current. The WPE initially increased rapidly before gradually decreasing as the current increased. When the current reached the threshold, the photons gener-

ated by electron-hole radiation recombination in the active region offset the lost photons. As the current increased, the efficiency of radiation recombination further increased, resulting in a rapid increase in the WPE. With a further increase in the current, the radiation recombination of carriers in the active region reached saturation. A further increase in the current caused overflow and nonradiative recombination of carriers in the active region, resulting in a decrease in the WPE. Therefore, the WPE initially increased rapidly and then decreased gradually. Structure D exhibited the highest WPE, highlighting the advantages of energy and high efficiency.

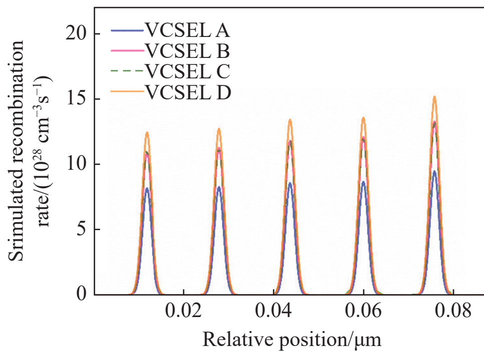

Fig. 5 Stimulated recombination rates in the active region for different structures at 20 mA

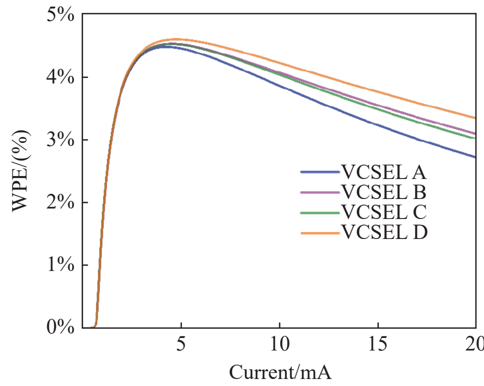

Fig. 6 Relationship between WPE and the injection current

To illustrate the underlying reasons for the enhancement of hole concentration in the MQW and the suppression of electron leakage in the hole-injection layer, we present band diagrams for the active region, EBL, and hole-injection layer of each structure (Figure 7). We defined the effective barrier height for carriers by considering the energy difference between the quasi-Fermi level of electrons and the conduction band as the electron barrier height and the energy difference between the quasi-Fermi level of holes and the valence band as the hole barrier height. First, the electron barrier heights for the structures were 141, 172, 190, and 193 meV, and the changes in these heights were analysed. A lower electron barrier height facilitates the escape of electrons from the active region to the p-type region, whereas a higher electron barrier height causes less electron leakage. Because of significant changes in the material composition near the electronic barrier layer, piezoelectric and polarisation effects are comparatively strong, resulting in band bending[38]. Band bending leads to a significant separation of the wave functions of holes and electrons, not only weakening the confinement of electrons in the active region but also limiting the injection of holes from the p-type layer[39].

Compared with structure A, the electron barrier height in structure B significantly increased after introducing polarisation doping. This is because the polarisation doping introduces bulk polarisation charges that can shield the polarisation-induced electric field in the QWs, reducing the quantum-confined Stark effect (QCSE). A decrease in the strength of the polarisation-induced electric field in the QW can increase the overlap of the electron-hole wavefunctions. The reduced QCSE is conducive to the stimulated radiative recombination of electrons and holes. The electron barrier height in structure C was also higher than that in structure A, indicating that the EBL structure could reduce electron leakage more effectively. Structure D had the maximum electron barrier height, indicating its superior ability to block electron leakage. This is consistent with the analysis of the electron concentration and electron current density distributions previously discussed.

Subsequently, the variation in the hole barrier height was analysed. The hole barrier heights for the structures were 170, 156, 167, and 147 meV, respectively. Structures B, C, and D had lower hole barrier heights than structure A. Specifically, struc-

ture D eliminated the abrupt barrier between the EBL and the HIL by changing the Al compositions of the EBL and HIL. This smoothens the valence band and facilitates hole injection, consistent with the previous analysis of the hole concentration and hole current density distributions.

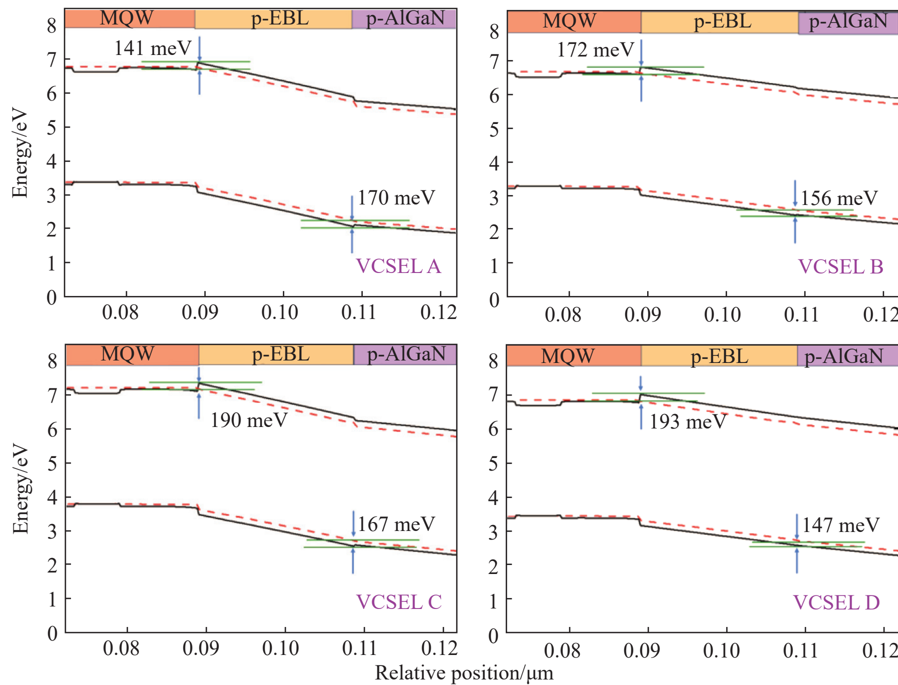

Fig. 7 Energy band diagrams of the active region and p-type doping regions of structures A, B, C, and D at 20 mA

4 Conclusion

We designed a GaN-based UV VCSEL structure and thoroughly investigated the combined effects of the gradient Al composition in the HIL and Al-composition gradient EBL on the device performance. Our results indicate that under the condition of a constant average Al composition in each structure, polarisation doping can introduce bulk polarisation charges to shield the polarisation-induced electric field in the QWs, reduce the QCSE, improve the hole injection efficiency, and enhance the ionisation efficiency of Mg dopants, thereby increasing the hole concentration. Furthermore, implementing an Al composition gradient in the EBL on this basis eliminates the abrupt hole barrier at the interface between the hole-injection layer and the EBL, smoothening the valence band. Moreover, the ability to block electron leakage is improved, suppressing unintentional hole-blocking layers. This approach effectively optimises the hole injection efficiency, increases the stimulated radiation recombination rate in the QW, decreases the threshold voltage, and achieves superior optoelectronic performance.

Acknowledgements

This work was supported by the Shanxi-Zheda Institute of Advanced Materials and Chemical Engineering (Grant Nos. 2021SX-AT002 and 2022SX-TD018), the Key R&D Projects in Shanxi Province (Grant No. 202302150101012), and the National Natural Science Foundation of China (Grant Nos. 61604104, 21972103, and 61904120). We would like to thank Editage (www.editage.cn) for English language editing.

Conflicts of interest

The authors declare no conflict of interest.

References:

[1] TAKEUCHI T, KAMIYAMA S, IWAYA M, *et al*.. GaN-based vertical-cavity surface-emitting lasers with AlInN/GaN distributed Bragg reflectors[J]. *Reports on Progress in Physics*, 2019, 82(1): 012502.

[2] CHEN Y H, MEI Y, ZHENG ZH M, *et al*.. Effects of different current confinement layers in GaN-based VCSELs[J]. *AIP Advances*, 2023, 13(7): 075114.

[3] XU R B, MEI Y, XU H, *et al*.. Effects of lateral optical confinement in GaN VCSELs with double dielectric DBRs[J]. *IEEE Photonics Journal*, 2020, 12(2): 1501708.

[4] ELAFANDY R T, KANG J H, MI CH Z Y, *et al*.. Study and application of birefringent nanoporous GaN in the polarization control of blue vertical-cavity surface-emitting lasers[J]. *ACS Photonics*, 2021, 8(4): 1041-1047.

[5] ELAFANDY R T, KANG J H, LI B J, *et al*.. Room-temperature operation of c-plane GaN vertical cavity surface emitting laser on conductive nanoporous distributed Bragg reflector[J]. *Applied Physics Lettrers*, 2020, 117(1): 011101.

[6] HAYASHI K, HAMAGUCHI T, KEARNS J A, *et al*.. Narrow emission of blue GaN-based vertical-cavity surface-emitting lasers with a curved mirror[J]. *IEEE Photonics Jouranl*, 2022, 14(4): 1536905.

[7] LEONARD J T, YOUNG E C, YONKEE B P, *et al*.. Comparison of nonpolar III-nitride vertical-cavity surface-emitting lasers with tunnel junction and ITO intracavity contacts[J]. *Proceedings of SPIE*, 2016, 9748: 97481B.

[8] YANG J, ZHAO D G, LIU Z SH, *et al*.. Room temperature continuous-wave operated 2.0-W GaN-based ultraviolet laser diodes[J]. *Optics Letters*, 2022, 47(7): 1666-1668.

[9] YANG J, ZHAO D G, LIU Z SH, *et al*.. A 357.9 nm GaN/AlGaN multiple quantum well ultraviolet laser diode[J]. *Jouranl of Semiconductors*, 2022, 43(1): 010501.

[10] ZHENG ZH M, WANG Y K, HOO J, *et al*.. High-quality AlGaN epitaxial structures and realization of UVC vertical-cavity surface-emitting lasers[J]. *Science China Materials*, 2023, 66(5): 1978-1988.

[11] WANG Y K, ZHENG ZH M, LONG H, *et al*.. Development and challenges of nitride vertical-cavity surface-emitting lasers (invited)[J]. *Acta Photonica Sinica*, 2022, 51(2): 0251203.

[12] QIU X J, ZHANG Y H, HANG SH, *et al*.. Enhancing the lateral current injection by modulating the doping type in the p-type hole injection layer for InGaN/GaN vertical cavity surface emitting lasers[J]. *Optics Express*, 2020, 28(12): 18035-18048.

[13] HAN L, GAO Y B, HANG SH, *et al*.. Impact of p-AlGaN/GaN hole injection layer on GaN-based vertical cavity surface emitting laser diodes [invited][J]. *Chinese Optics Letters*, 2022, 20(3): 031402.

[14] PENG F, YANG CH, DENG S Y, *et al*.. Simulation of a high-performance enhancement-mode HFET with back-to-back graded AlGaN layers[J]. *Science China Information Sciences*, 2019, 62(6): 62403.

[15] VERMA J, ISLAM S M, PROTASENKO V, *et al*.. Tunnel-injection quantum dot deep-ultraviolet light-emitting diodes with polarization-induced doping in III-nitride heterostructures[J]. *Applied Physics Letters*, 2014, 104(2): 021105.

[16] ZHANG L, DING K, YAN J C, *et al*.. Three-dimensional hole gas induced by polarization in (0001)-oriented metal-face III-nitride structure[J]. *Applied Physics Letters*, 2010, 97(6): 062103.

[17] ZHANG H CH, HUANG CH, SONG K, *et al*.. Compositionally graded III-nitride alloys: building blocks for efficient ultraviolet optoelectronics and power electronics[J]. *Reports on Progress in Physics*, 2021, 84(4): 044401.

[18] XING ZH Y, ZHANG H CH, SUN Y, *et al*.. Normally-OFF AlGaN/GaN-based HEMTs with decreasingly graded AlGaN cap layer[J]. *Journal of Physics D: Applied Physics*, 2023, 56(2): 025105.

[19] ZHANG H CH, LIANG F ZH, YANG L, *et al*.. Superior AlGaN/GaN-based phototransistors and arrays with reconfigurable triple-mode functionalities enabled by voltage-programmed two-dimensional electron gas for high-quality imaging[J]. *Advanced Materials*, 2024, 36(36): 2405874.

[20] KOLBE T, KNAUER A, RASS J, *et al*.. 234 nm far-ultraviolet-C light-emitting diodes with polarization-doped hole injection layer[J]. *Applied Physics Letters*, 2023, 122(19): 191101.

[21] SATTER M, LOCHNER Z, KAO T T, *et al*.. AlGaN-based vertical injection laser diodes using inverse tapered p-waveguide for efficient hole transport[J]. *IEEE Journal of Quantum Electronics*, 2014, 50(3): 166-173.

[22] LIU Y S, KAO T T, SATTER M, *et al*.. Inverse-tapered p-waveguide for vertical hole transport in high-[Al] AlGaN emitters[J]. *IEEE Photonics Technology Letters*, 2015, 27(16): 1768-1771.

[23] LU L, DING G G, ZHANG Y, *et al*.. Improved performance of AlGaN-based deep ultraviolet light-emitting diode using

modulated-taper design for p-AlGaN layer[J]. *Semiconductor Science and Technology*, 2018, 33(3): 035008.

[24] LUO H W, LI J Z, LI M. Improved output power of GaN-based VCSEL with band-engineered electron blocking layer[J]. *Micromachines*, 2019, 10(10): 694.

[25] CHENG CH, LEI Y, LIU ZH Q, *et al*.. Performance improvement of light-emitting diodes with double superlattices confinement layer[J]. *Journal of Semiconductors*, 2018, 39(11): 114005.

[26] MONDAL R K, CHATTERJEE V, PAL S. Effect of step-graded superlattice electron blocking layer on performance of AlGaN based deep-UV light emitting diodes[J]. *Physica E: Low-Dimensional Systems and Nanostructures*, 2019, 108: 233-237.

[27] YANG W, LI D, LIU N Y, *et al*.. Improvement of hole injection and electron overflow by a tapered AlGaN electron blocking layer in InGaN-based blue laser diodes[J]. *Applied Physics Letters*, 2012, 100(3): 031105.

[28] WANG Y F, NIASS M I, WANG F, *et al*.. Improvement of radiative recombination rate in deep ultraviolet laser diodes with step-like quantum barrier and aluminum-content graded electron blocking layer[J]. *Chinese Physics B*, 2020, 29(1): 017301.

[29] AZOFF E M. Closed-form method for solving the steady-state generalised energy-momentum conservation equations[J]. *COMPEL - The International Journal for Computation and Mathematics in Electrical and Electronic Engineering*, 1987, 6(1): 25-30.

[30] TURIN V O. A modified transferred-electron high-field mobility model for GaN devices simulation[J]. *Solid-State Electronics*, 2005, 49(10): 1678-1682.

[31] PELA R R, HSIAO C L, HULTMAN L, *et al*.. Electronic and optical properties of core-shell InAlN nanorods: a comparative study *via* LDA, LDA-1/2, mBJ, HSE06, G_0W_0 and BSE methods[J]. *Physical Chemistry Chemical Physics*, 2024, 26(9): 7504-7514.

[32] CHUANG CH M, CHENG Y H, WU Y R. Electro-optical numerical modeling for the design of UVA nitride-based vertical-cavity surface-emitting laser diodes[J]. *IEEE Journal of Selected Topics in Quantum Electronics*, 2022, 28(1): 1700606.

[33] LAI C Y, HSU T M, CHANG W H, *et al*.. Direct measurement of piezoelectric field in $In_{0.23}Ga_{0.77}N$/GaN multiple quantum wells by electrotransmission spectroscopy[J]. *Journal of Applied Physics*, 2002, 91(1): 531-533.

[34] GAO Y B, CHU CH SH, HANG SH, *et al*.. Quantum barriers with a polarization self-screening effect for GaN-based VCSELs to increase the electron-hole stimulated recombination and output performance[J]. *Optical Materials Express*, 2021, 11(12): 3984-3995.

[35] HADLEY G R, LEAR K L, WARREN M E, *et al*.. Comprehensive numerical modeling of vertical-cavity surface-emitting lasers[J]. *IEEE Journal of Quantum Electronics*, 1996, 32(4): 607-616.

[36] HAN S H, LEE D Y, LEE S J, *et al*.. Effect of electron blocking layer on efficiency droop in InGaN/GaN multiple quantum well light-emitting diodes[J]. *Applied Physics Letters*, 2009, 94(23): 231123.

[37] LI SH B, WARE M, WU J, *et al*.. Polarization induced pn-junction without dopant in graded AlGaN coherently strained on GaN[J]. *Applied Physics Letters*, 2012, 101(12): 122103.

[38] BAO X L, SUN P, LIU S Q, *et al*.. Performance improvements for AlGaN-based deep ultraviolet light-emitting diodes with the p-type and thickened last quantum barrier[J]. *IEEE Photonics Journal*, 2015, 7(1): 1400110.

[39] SI Q Y, CHEN H Y, LI SH P, *et al*.. Improved characteristics of AlGaN-based deep ultraviolet light-emitting diodes with superlattice p-type doping[J]. *IEEE Photonics Journal*, 2017, 9(3): 2200807.

Author Biographics：

WEN Xin-xin (1999 —), M.Sc, Key Laboratory of Interface Science and Engineering in Advanced Materials Ministry of Education, Taiyuan University of Technology. Her research focuses on optoelectronic materials and devices. E-mail: wxx2583692024@163.com

JIA Wei (1983—), Ph.D., Senior Experimentalist, Master's Supervisor, Key Laboratory of Interface Science and Engineering in Advanced Materials Ministry of Education, Taiyuan University of Technology. His main research focuses on semiconductor optoelectronic materials and devices. E-mail: jiawei@tyut.edu.cn